

Combined hardening and localized failure with softening plasticity in dynamics

Xuan Nam Do^{1a}, Adnan Ibrahimbegovic^{*1,2} and Delphine Brancherie^{1b}

¹Université de Technologie Compiègne / Sorbonne Universités, Laboratoire Roberval de Mécanique
Centre de Recherche Royallieu, Rue Personne de Roberval, 60200 Compiègne, France

²Chair for Computational Mechanics, Computational Mechanics

(Received April 10, 2015, Revised June 7, 2015, Accepted June 9, 2015)

Abstract. We present for one-dimensional model for elastoplastic bar with combined hardening in FPZ - fracture process zone and softening with embedded strong discontinuities. The simplified version of the model without FPZ is directly compared and validated against analytical solution of Bazant and Belytschko (1985). It is shown that deformation localizes in an area which is governed by the chosen element size and therefore causes mesh sensitivity and that the length of the strain-softening region tends to localize into a point, which also agrees with results obtained by stability analysis for static case. Strain increases in the softening domain with a simultaneous decrease of stress. The problem unloads elastically outside the strain-softening region. The more general case with FPZ leads to more interesting results that also account for induced strain heterogeneities.

Keywords: dynamics; FPZ - fracture process zone; strain-softening; localization; finite element; embedded discontinuity

1. Introduction

The development of localized deformation is caused by a failure process at the material's microscale. The microscopic behavior is governed by growth, interaction and coalescence of microcracks which eventually results in complete fracture and softening at the macroscale. In a structural concrete member micro-cracking leads to a local decrease in the effective cross-sectional area that transmits tensile forces. This phenomenon is commonly called softening and is accompanied by the formation of narrow bands of intense straining (localization of deformation). In addition, according to Rudnicki and Rice (1975): "localization can be understood as instability in the macroscopic constitutive description of inelastic deformation of the material". The instability allows the constitutive equations of an originally homogeneous material to reach a bifurcation point where the non-uniform deformation localizes. Outside this localization zone the material continues to unload elastically. Throughout this process the body remains in dynamic equilibrium expressed in terms of the d'Alembert principle.

*Corresponding author, Professor, E-mail: adnan.ibrahimbegovic@utc.fr

^aE-mail: xuan-nam.do@utc.fr

^bE-mail: delphine.brancherie@utc.fr

The strain softening of a material is the decline of stress at increasing strain and represents the process of progressive failure or damage. The dynamic strain-softening problem is highly nonlinear leading to instability (Similar problems of instability also occur for geometric instabilities (Ibrahimbegovic, Hajdo and Dolarevic (2013), Ngo, Ibrahimbegovic and Hajdo (2014)). An analytical solution for a one-dimensional wave propagation problem was derived by Bazant and Belytschko (1985) for the simplest case of elastic-softening response. Fig. 1 shows the stress-strain curve of such a strain-softening material. The linear elastic area is shown between the points O & P. The stiffness is given by Young's modulus E . The maximum strength f'_t is reached for the plastic strain ϵ_p . The curve in the strain-softening area (area between points P and F) is given by the function $F(\epsilon)$. The slope of this curve, $F'(\epsilon)$, is negative. $F(\epsilon)$ reaches a zero stress value for a finite strain ϵ or an asymptotic strain $\epsilon \rightarrow \infty$. Unloading ($\dot{\epsilon} < 0$) and reloading ($\dot{\epsilon} \geq 0$) is considered to be elastic and happens with Young's modulus E of the linear elastic area.

In order to compare with analytical solution of Bazant and Belytschko (1985), we present a discrete bar model with strong discontinuities that are embedded into the finite elements through the proper enhancement of the discrete strain field of the element. This developed model is one-dimensional truss-bar capable of representing the dynamic fracture.

This paper aims to support the understanding of localized failure for this and more general case where strain-hardening and strain-softening elastoplastic behavior are combined in dynamics. The outline of the paper is as follows: In Section 2, we introduce the model theoretical formulation. A closed-form reference solution for a dynamic strain-softening problem is provided in Section 3 for a simple case with negligible FPZ. The numerical implementation for one-dimensional bar with embedded strong discontinuities will be discussed in Section 4. Section 5 presents numerical simulations for this and more general case including FPZ. Finally, conclusions are given in Section 6.

2. Theoretical formulation

2.1 Elastoplastic material behavior

For elastoplastic material behavior the strain increase is followed in general by the stress increase immediately but there may be a permanent deformation after stress release, Fig. 2.

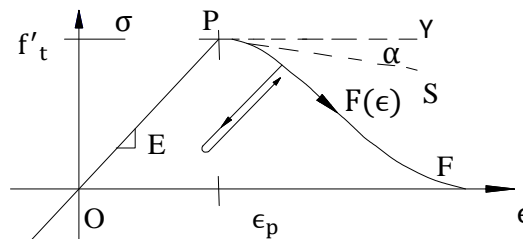


Fig. 1 Stress-strain diagram of elastic - strain-softening material

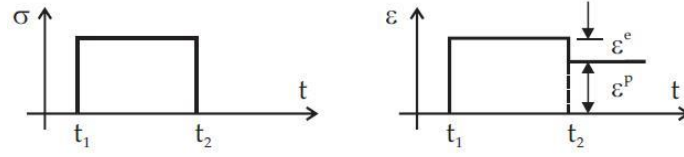


Fig. 2 Elastoplastic material behavior

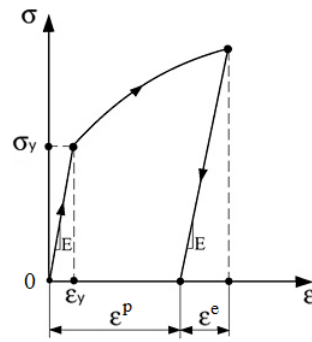


Fig. 3 Stress-strain response of strain-hardening material

2.2 Model for isotropic hardening plasticity

Real metallic materials exhibit a characteristics known as strain hardening. Strain hardening is the strengthening of a metal by accumulated plastic deformation. This strengthening occurs because of dislocation movements within the crystal structure of the material. The stress–strain curve for strain hardening material is shown in Fig. 3.

2.2.1 Assumptions, Observations, Definitions

(i) The total strain ε splits into an elastic part ε^e and a plastic part ε^p

$$\varepsilon = \varepsilon^e + \varepsilon^p \quad (1)$$

(ii) The stress σ is given by the linear elastic relationship

$$\sigma = E\varepsilon^e = E(\varepsilon - \varepsilon^p) \quad (2)$$

(iii) The set of admissible stresses is denoted by

$$\mathbb{E}_\sigma = \{\sigma \in \mathbb{R} \mid \Phi(\sigma, \xi) = |\sigma| - (\sigma_y + K\xi) \leq 0\} \quad (3)$$

where σ_y is called the flow stress or yield stress

$\Phi(\sigma, \xi)$ denotes the yield function

K refers to isotropic hardening modulus

ξ is the internal variable in which $\dot{\xi} = |\dot{\varepsilon}^p|$ is the simplest evolution equation for ξ

The center of \mathbb{E}_σ remains at the origin. The hardening is linear in the amount of plastic flow (linear in $|\varepsilon^p|$).

(iv) If $\Phi(\sigma, \xi) < 0$ no change in ε^p takes place, $\dot{\varepsilon}_p = 0$. The instantaneous response is governed by elastic regime. The elastic range is defined as the open set

$$\text{int}(\mathbb{E}_\sigma) = \{\sigma \in \mathbb{R} \mid \Phi(\sigma, \xi) = |\sigma| - (\sigma_y + K\xi) < 0\} \quad (4)$$

where the interior of \mathbb{E}_σ , denoted by $\text{int}(\mathbb{E}_\sigma)$, is referred to as the elastic domain

(v) A change in ε^p can take place only if $\Phi(\sigma, \xi) = 0$. If this condition is met the material experiences slip in the direction of the applied stress with constant slip rate $\dot{\gamma} \geq 0$

$$\dot{\varepsilon}^p = \begin{cases} +\dot{\gamma}, & \text{if } \sigma = +\sigma_y > 0 \\ -\dot{\gamma}, & \text{if } \sigma = -\sigma_y < 0 \end{cases} \quad (5)$$

These cases can be recast into the following single equation

$$\dot{\varepsilon}^p = \dot{\gamma} \text{sign}(\sigma) \text{ if } \Phi(\sigma, \xi) = 0, \quad (6)$$

which goes by the name of flow rule. The sign-function is defined by

$$\text{sign}(x) = \begin{cases} +1, & \text{if } x > 0 \\ -1, & \text{if } x < 0 \end{cases} \quad (7)$$

The boundary of the elastic range \mathbb{E}_σ , denoted by $\partial\mathbb{E}_\sigma$, is referred to as the yield surface in stress space

$$\partial\mathbb{E}_\sigma = \{\sigma \in \mathbb{R} \mid \Phi(\sigma, \xi) = |\sigma| - (\sigma_y + K\xi) = 0\} \quad (8)$$

(vi) The evolution of ε^p can be completely described with the evolution equation $\dot{\varepsilon}^p = \dot{\gamma} \text{sign}(\sigma)$ provided that $\dot{\gamma}$ and σ are restricted by certain unilateral constraints:

a) σ must be admissible, that is $\sigma \in \mathbb{E}_\sigma$, and $\dot{\gamma}$ must be nonnegative

$$\dot{\gamma} \geq 0 \quad \text{and} \quad \Phi(\sigma, \xi) \leq 0 \quad (9)$$

b) $\dot{\gamma} = 0$ if $\Phi(\sigma, \xi) < 0$ and $\dot{\gamma} > 0$ only if $\Phi(\sigma, \xi) = 0$. It follows

$$\dot{\gamma} \Phi(\sigma, \xi) = 0 \quad (10)$$

c) Consistency condition: $\dot{\gamma} > 0 \Rightarrow \dot{\Phi} = 0$ and $\dot{\Phi} < 0 \Rightarrow \dot{\gamma} = 0$, which can be recast into the single condition

$$\dot{\gamma} \dot{\Phi}(\sigma, \xi) = 0 \quad (11)$$

Condition (a) and (b) go by the name Kuhn-Tucker complementary conditions

2.2.2 Model summary

One-dimensional rate-independent plasticity with isotropic hardening

- Constitutive relation

$$\sigma = E(\varepsilon - \varepsilon^p) \quad (12)$$

- Plastic flow rule

$$\dot{\varepsilon}^p = \dot{\gamma} \text{sign}(\sigma) \quad (13)$$

- Isotropic hardening evolution law

$$\dot{\xi} = |\dot{\varepsilon}^p| = \dot{\gamma} \quad (14)$$

- Yield function

$$\Phi(\sigma, \xi) = |\sigma| - (\sigma_y + K\xi) \leq 0 \quad (15)$$

- Kuhn-Tucker complementary conditions (loading-unloading conditions)

$$\dot{\gamma} > 0 \Phi(\sigma, \xi) \leq 0 \dot{\gamma} \Phi(\sigma, \xi) = 0 \quad (16)$$

- Consistency condition

$$\dot{\gamma} \dot{\Phi}(\sigma, \xi) = 0 \quad (17)$$

2.2.3 Stress-strain rate form

The complementary condition $\dot{\gamma} \Phi < 0$ implies that when $\Phi < 0$ we will have $\dot{\gamma} = 0$ and when $\dot{\gamma} > 0$ we will have $\Phi = 0$.

In the first case $\dot{\gamma} = 0$ the material shows instantaneous elastic response. Thus $\dot{\varepsilon}_p = 0$ and we obtain the rate form $\dot{\sigma} = E\dot{\varepsilon}$.

In the second case $\dot{\gamma} > 0$ and consequently $\Phi = 0$. Because $\Phi = 0$ remains constant as long as $\dot{\gamma} > 0$ also the rate of Φ vanishes, $\dot{\Phi} = 0$, and we obtain

$$\begin{aligned} \dot{\Phi} &= \frac{\partial \Phi}{\partial \sigma} \dot{\sigma} + \frac{\partial \Phi}{\partial \xi} \dot{\xi} \\ &= \text{sign}(\sigma) E (\dot{\varepsilon} - \dot{\varepsilon}^p) - K \dot{\xi} \\ &= \text{sign}(\sigma) E \dot{\varepsilon} - \dot{\varepsilon}^p \text{sign}(\sigma) E - K \dot{\gamma} \Rightarrow \dot{\gamma} = \frac{E}{E+K} \dot{\varepsilon} \text{sign}(\sigma) \\ &= \text{sign}(\sigma) E \dot{\varepsilon} - \dot{\gamma} \text{sign}(\sigma) \text{sign}(\sigma) E - K \dot{\gamma} \\ &= \text{sign}(\sigma) E \dot{\varepsilon} - \dot{\gamma} (E + K) = 0 \end{aligned} \quad (18)$$

$$\dot{\varepsilon}^p = \dot{\gamma} \text{sign}(\sigma) = \frac{E}{E+K} \dot{\varepsilon} \quad (19)$$

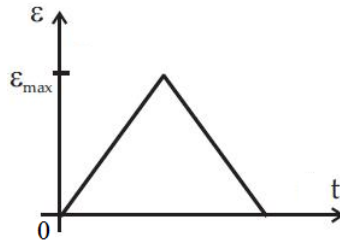


Fig. 4 Stress-time function

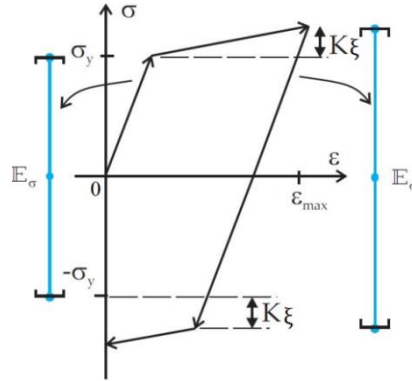


Fig. 5 Stress-strain curve of the isotropic hardening model

Hence, we obtain the following form for stress rate equation

$$\dot{\sigma} = \begin{cases} E \dot{\epsilon} ; \dot{\gamma} = 0 \\ \frac{EK}{E+K} \dot{\epsilon} ; \dot{\gamma} > 0 \end{cases} \quad (20)$$

The stress response of a body subjected to the strain-time function shown in Fig. 4 is given in Fig. 5.

3. Reference solution in a bar – analytical solution of dynamic strain-softening

Consider a bar of length $2L$, with a unit cross-sectional area and a density ρ per unit length. Let the bar be loaded by forcing both ends to move simultaneously outward, with constant opposite velocities of magnitude v . The longitudinal coordinate x is measured from the bar's center (Fig. 6). The boundary conditions are

$$\begin{cases} \text{For } x = -L: u = -vt \\ \text{For } x = L: u = vt \end{cases} \quad (\text{for } t \geq 0) \quad (21)$$

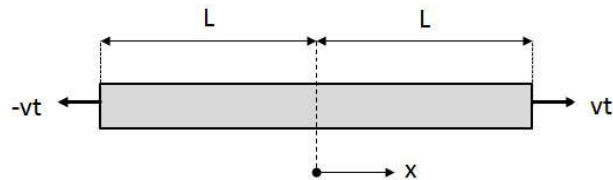


Fig. 6 Geometry and loading of strain-softening bar

Two step waves are generated in the bar. One wave travels from the right boundary in the negative x -direction. The other wave travels from the left boundary in the positive x -direction. The two step waves of constant strain travel to the center of the bar and meet $x = 0$ for the time $t = L/c_e$. When the two waves meet strain doubles instantaneously at the center of the bar if $\varepsilon \leq \varepsilon_p/2$ and the midsection enters immediately the strain-softening regime with an increase to infinite strain if $\varepsilon_p/2 < \varepsilon \leq \varepsilon_p$.

Before the onset of strain-softening the problem is governed by the differential equation of motion with the elastic wave speed $c_e = \sqrt{\frac{E}{\rho}}$. This standard equation is the wave equation, which is hyperbolic for real wave speeds.

$$c_e^2 \frac{\partial^2 u}{\partial x^2} = \frac{\partial^2 u}{\partial t^2} \quad (22)$$

The longitudinal displacement function in the linear elastic domain is derived from appropriate initial and boundary conditions.

$$u(x, t) = -v \left\langle t - \frac{x+L}{c_e} \right\rangle + v \left\langle t + \frac{x-L}{c_e} \right\rangle \quad (23)$$

in which the symbol $\langle \ \rangle$ is defined as $\langle A \rangle = A$ if $A > 0$ and $\langle A \rangle = 0$ if $A \leq 0$

The corresponding strain function needs to be positive. Accordingly, the Heaviside step function H is used.

$$\varepsilon = \frac{\partial u}{\partial x} = \frac{v}{c_e} \left[H \left(t - \frac{x+L}{c_e} \right) + H \left(t + \frac{x-L}{c_e} \right) \right] \quad (24)$$

The stress caused by the deformation is described with Hooke's law for linear elasticity.

$$\sigma = E\varepsilon \quad (25)$$

Obviously, if $\varepsilon \leq \varepsilon_p/2$, the assumption of elastic behavior holds for $t \leq 2L/c_e$, i.e., until the time each wave-front runs the entire length of the bar. If, however, $\varepsilon_p/2 < \varepsilon \leq \varepsilon_p$, the solution for the displacement $u(x, t)$ in Eq. (23) holds only for $t \leq L/c_e$.

The slope of the stress-strain diagram in the strain-softening domain is $F'(\varepsilon)$ that is less than zero. Because $F'(\varepsilon) < 0$, the differential equation of motion in the strain-softening domain is elliptic, which means that interaction over finite distances is immediate.

$$c_e^2 \frac{\partial^2 u}{\partial x^2} + \frac{\partial^2 u}{\partial t^2} = 0 \quad \text{with } c_e^2 = \frac{F'(\varepsilon)}{\rho} \quad (26)$$

Strain-softening is limited to an area around $x = 0$. The displacements develop a discontinuity at $x = 0$, with a jump of magnitude $4v \langle t - L/c_e \rangle$. Strain starts to increase infinitely and stress drops to zero in the strain-softening zone. The rest of the bar starts to unload elastically.

Strain near $x = 0$, i.e., at the center of the bar can be expressed by the Dirac Delta function

$$\varepsilon = 4v \langle t - L/c_e \rangle \delta(x) \quad (27)$$

The solution for the strain field outside the strain – softening zone, $t > L/c_e$ and $x < 0$, is

$$\varepsilon = \frac{v}{c_e} \left[H \left(t - \frac{x+L}{c_e} \right) + H \left(t + \frac{x-L}{c_e} \right) + 4v \langle t - L/c_e \rangle \delta(x) \right] \quad (28)$$

For the right half of the bar, $x > 0$, a symmetric solution applies.

4. Numerical implementation: finite element with embedded strong discontinuities

4.1 Standard finite element interpolation

The displacement interpolation for one-dimensional truss bar with 2 nodes can be written as

$$u(x) = \sum_{a=1}^2 N_a(x)u_a = \mathbf{N}\mathbf{u} \quad (29)$$

where \mathbf{u} represents nodal displacement vectors.

For this case of element, we use standard linear interpolation functions for continuum displacement approximation

$$\mathbf{N} = \left\{ N_1(x) = 1 - \frac{x}{l^e}, N_2(x) = \frac{x}{l^e} \right\} \quad (30)$$

The strain interpolation can be obtained from the displacement field resulting in

$$\varepsilon(x) = \frac{du(x)}{dx} = \mathbf{B}\mathbf{u} \quad (31)$$

where \mathbf{B} is the strain-displacement matrix

$$\mathbf{B} = \frac{d\mathbf{N}}{dx} = \frac{1}{l^e} [-1 \ 1] \quad (32)$$

4.2 Strong discontinuity kinematics

Once the localized failure occurs, the crack opening (further denoted as α , see Fig. 8) contributes to a “jump” or irregular part in the displacement field. Thus, the total displacement field is the sum of regular (smooth) part and irregular part.

$$u(x, t) = \hat{u}(x, t) + \alpha \{ H_{x_c}(x) - \varphi(x) \} \quad (33)$$

$$u(x, t) = \hat{u}(x, t) - \alpha \varphi(x) + \alpha H_{x_c}(x) \quad (34)$$

where $H_{x_c}(x)$ is the Heaviside function introducing the displacement jump.

$$H_{x_c}(x) = \begin{cases} 1; & x > x_c \\ 0; & x < x_c \end{cases} \quad (35)$$

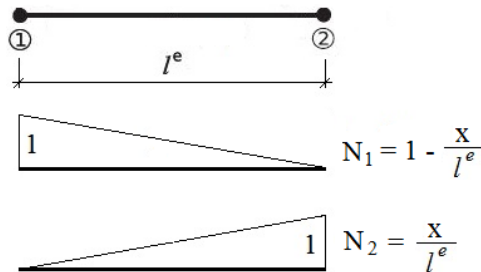


Fig. 7 Shape function

and $\varphi(x)$ is a (smooth) function, introduced to limit the influence of the displacement jump within the “failure” domain. Usual choice for $\varphi(x)$ in the finite element implementation pertains to the shape function of selected interpolation. For a 1D truss-bar with 2 nodes, we can choose

$$\varphi(x) = N_2(x) = \frac{x}{l^e} \quad (36)$$

The corresponding illustrations for $H_{x_c}(x)$ and $\varphi(x)$ for a two-node truss-bar element are given in Fig. 9.

Denoting with $\bar{u}(x, t) = \hat{u}(x, t) - \alpha\varphi(x)$ the continuous part of the displacement field, and with α the “jump” in displacement, we can further write additive decomposition of displacement field:

$$u(x, t) = \bar{u}(x, t) + \alpha H_{x_c}(x) \quad (37)$$

$$u(x, t) = \bar{u}(x, t) + \alpha\varphi(x) + \underbrace{\alpha\{H_{x_c}(x) - \varphi(x)\}}_{M(x)} \quad (38)$$

$$u(x, t) = \bar{u}(x, t) + \alpha N_2(x) + \alpha\{H_{x_c}(x) - N_2(x)\} \quad (39)$$

In Eq. (38) above, $M(x)$ is the additional interpolation function (see Fig. 9), and can be used alongside standard interpolation function to describe the heterogeneous displacement field with activated jump inside the finite element. The $M(x)$ is defined as follows

$$M(x) = \begin{cases} -\frac{x}{l^e}; & x \in [0, x_c) \\ 1 - \frac{x}{l^e}; & x \in \langle x_c, l^e] \end{cases} \quad (40)$$

The finite element displacement interpolation can thus be stated as

$$u(x) = \sum_{a=1}^2 N_a(x)u_a + \alpha M(x) \quad (41)$$

The corresponding strain field can then be obtained by exploiting the kinematic relation

$$\varepsilon(x, t) = \sum_{a=1}^2 B_a(x)u_a + \alpha G(x) \quad (42)$$

where

$$G(x) = G + \delta_{x_c} = -\frac{1}{l^e} + \delta_{x_c}, x \in [0, l^e] \quad (43)$$

and

$$\delta_{x_c} = \begin{cases} \infty; & x = x_c \\ 0; & \text{otherwise} \end{cases} \text{ - Dirac's Delta function} \quad (44)$$

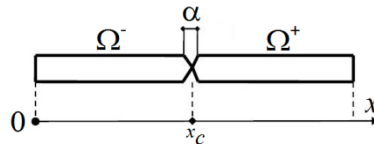


Fig. 8 Displacement discontinuity at localized failure for the mechanical load

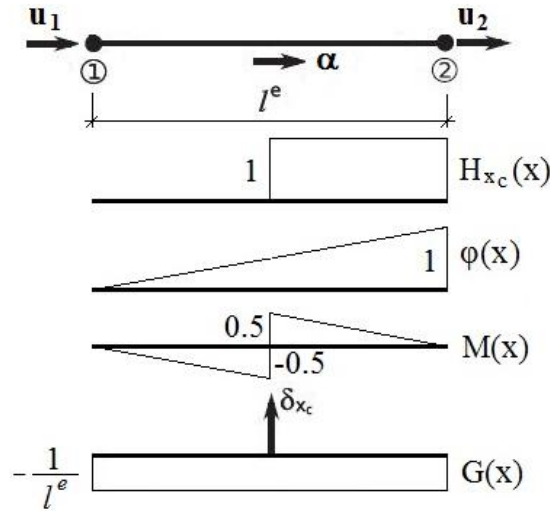


Fig. 9 Displacement discontinuity for 2-node bar element: Heaviside function, smooth function and additional interpolation function

4.2 Computational procedure

The solution will be computed at discrete pseudo-time values $0, t_1, t_2, \dots, t$ by means of incremental iterative scheme. The local phase will be treated separately from global phase:

The local (element) computation should provide the values of internal variables at the end of time step guaranteeing the plastic admissibility of the stress field. Implicit backward Euler scheme will be taken for time integration of evolution equations.

Given: $d_{n+1}, \bar{\varepsilon}_n^p, \bar{\gamma}_n^p, \bar{\xi}_n, \alpha_n, \bar{\xi}_n, \Delta t = t_{n+1} - t_n$

Find: $\bar{\varepsilon}_{n+1}^p, \bar{\gamma}_{n+1}^p, \bar{\xi}_{n+1}, \alpha_{n+1}, \bar{\xi}_{n+1}$

In the global phase, we compute the current iterative values of nodal displacements at t_{n+1} while keeping other variables fixed.

Given: d_{n+1}, α_{n+1}

Find: $d_{n+1} = d_n + \Delta d_{n+1}$

The subscript n denotes the values of variables at the discrete pseudo time t_n . First, we need to solve the elastoplastic part of the task, and once passed the ultimate stress, deal with localized failure and the softening phase.

The local computation for the elastoplastic phase can be summarized in the following Return Mapping Algorithm:

Initial data: $\bar{\varepsilon}_n^p, \bar{\xi}_n$

Strain: $\varepsilon_{n+1} = \sum_{a=1}^2 \mathbf{B}_a d_{a,n+1}$

Compute elastic trial stress and test for plastic loading

$$\sigma_{n+1}^{\text{trial}} = E(\varepsilon_{n+1} - \bar{\varepsilon}_n^p) \quad (45)$$

$$\bar{\Phi}_{n+1}^{\text{trial}} = |\sigma_{n+1}^{\text{trial}}| - \left(\sigma_y + \underbrace{K\bar{\xi}_n}_{-\bar{q}_n} \right) \quad (46)$$

If $\bar{\Phi}_{n+1}^{\text{trial}} \leq 0$ then

Elastic step: $\sigma_{n+1} = \sigma_{n+1}^{\text{trial}}; C = E \quad (47)$

Exit

Else

$$\bar{\gamma}_{n+1} = \frac{\bar{\Phi}_{n+1}^{\text{trial}}}{E+K} \quad (48)$$

$$\bar{\varepsilon}_{n+1}^p = \bar{\varepsilon}_n^p + \bar{\gamma}_{n+1} \text{sign}(\sigma_{n+1}^{\text{trial}}) \quad (49)$$

$$\bar{\xi}_{n+1} = \bar{\xi}_n + \bar{\gamma}_{n+1} \quad (50)$$

$$\sigma_{n+1} = E(\varepsilon_{n+1} - \bar{\varepsilon}_{n+1}^p) \quad (51)$$

$$C = \frac{EK}{E+K} \quad (52)$$

End

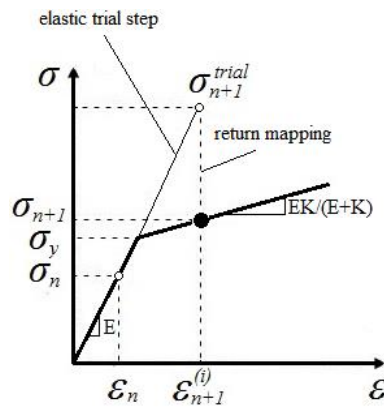


Fig. 10 Return mapping algorithm

Once the ultimate stress σ_u is reached, we carry on with solving the softening part of the task. Similar to hardening part, the local computation for this phase is summarized in the Return Mapping Algorithm as follows:

Initial data: $\bar{\varepsilon}_p, \alpha_n$

Compute elastic trial traction force and test for plastic loading

$$t_{n+1}^{\text{trial}} = E(\varepsilon_{n+1} - \bar{\varepsilon}_p + \bar{G}\alpha_n) \quad (53)$$

$$\bar{\Phi}_{n+1}^{\text{trial}} = |t_{n+1}^{\text{trial}}| - \left(\sigma_u + K_s \bar{\xi}_n \right) - \bar{q}_n \quad (54)$$

If $\bar{\Phi}_{n+1}^{\text{trial}} \leq 0$ then

Elastic step: $t_{n+1} = t_{n+1}^{\text{trial}}$ (55) Exit

Else

$$\bar{\gamma}_{n+1} = \frac{\bar{\Phi}_{n+1}^{\text{trial}}}{\frac{E}{l^e} + K_s} \quad (56)$$

$$\alpha_{n+1} = \alpha_n + \bar{\gamma}_{n+1} \text{sign}(t_{n+1}^{\text{trial}}) \quad (57)$$

$$\bar{\xi}_{n+1} = \bar{\xi}_n + \bar{\gamma}_{n+1} \quad (58)$$

$$t_{n+1} = t_{n+1}^{\text{trial}} - \frac{E}{l^e} \bar{\gamma}_{n+1} \text{sign}(t_{n+1}^{\text{trial}}) \quad (59)$$

End

After the local computation is finished and the values of internal variables obtained, we turn to the global phase in order to provide new iterative values of nodal displacements. In this phase, we consider the numerical simulations by implicit Newmark scheme and Newton-Raphson method.

The system of linearized equations can be written as

$$\begin{bmatrix} \mathbb{A}_{e=1}^{nel} \hat{\mathbf{K}}^{(e)} & \mathbb{A}_{e=1}^{nel} \mathbf{F}^{(e)} \\ \mathbf{F}^{(e),T} & \mathbf{H}^{(e)} \end{bmatrix}_{n+1}^i \begin{pmatrix} \Delta \mathbf{d}_{n+1}^{(e),(t)} \\ \Delta \alpha_{n+1}^{(e),(t)} \end{pmatrix} = \begin{pmatrix} \mathbb{A}_{e=1}^{nel} \mathbf{r}_{n+1}^{(e),(t)} \\ \mathbf{h}_{n+1}^{(e),(t)} \end{pmatrix} \quad (60)$$

in which the parts of element stiffness matrix are as follows

$$\hat{\mathbf{K}}^{(e)} = \mathbf{K}^{(e)} + \frac{1}{\beta(\Delta t)^2} \mathbf{M}^{(e)} \quad (61)$$

$$\mathbf{K}^{(e)} = \int_0^{l^e} \mathbf{B}^T \mathbf{C} \mathbf{B} dx \quad (62)$$

$$\mathbf{F}^{(e)} = \int_0^{l^e} \mathbf{B}^T \mathbf{C} \mathbf{G} dx \quad (63)$$

$$\mathbf{H}^{(e)} = \int_0^{l^e} \mathbf{G}^T \mathbf{C} \mathbf{G} dx + K_s \quad (64)$$

and $\mathbf{r}^{(e)}$ and $\mathbf{h}^{(e)}$ are residuals

$$\mathbf{r}^{(e)} = \mathbf{f}_{ext}^{(e)} - \mathbf{f}_{int}^{(e)} - \mathbf{M}^{(e)}\mathbf{a} \quad (65)$$

$$\mathbf{h}^{(e)} = \int_0^{l^e} \mathbf{G}^T \sigma dx + t \quad (66)$$

with t is the traction force acting at discontinuity.

In Eq. (61) above, $\mathbf{M}^{(e)}$ is the element mass matrix.

$$\mathbf{M}^{(e)} = \int_{\Omega} \rho \mathbf{N}^T \mathbf{N} d\Omega \quad (67)$$

and $\mathbf{f}_{ext}^{(e)}$ and $\mathbf{f}_{int}^{(e)}$ in Eq. (65) are external and internal force, respectively.

$$\mathbf{f}_{ext}^{(e)} = \int_{\Omega} \mathbf{N} \mathbf{b} \mathbf{N}^T d\Omega + [\mathbf{N}^T \bar{t}]_{\Gamma_{\sigma}} \quad (68)$$

$$\mathbf{f}_{int}^{(e)} = \int_{\Omega} \mathbf{B}^T \sigma d\Omega \quad (69)$$

4.3 Static condensation

One of the main features of finite element framework with embedded strong discontinuities is the ability to statically condense out the local element parameters on the element level, leaving the focus again on the solution of the global problem in terms of the global displacement field \mathbf{d} . Then, the final statically condensed system is:

$$\mathbb{A}_{e=1}^{nel} \left(\mathbf{K}_{eff,n+1}^{(e),(i)} \Delta \mathbf{d}_{n+1}^{(e),(i)} \right) = \mathbb{A}_{e=1}^{nel} \mathbf{r}_{eff,n+1}^{(e),(i)} \quad (70)$$

The effective stiffness matrix and effective residual of element are respectively defined by

$$\mathbf{K}_{eff}^{(e)} = \hat{\mathbf{K}}^{(e)} - \mathbf{F}^{(e)} (\mathbf{H}^{(e)})^{-1} \mathbf{F}^{(e),T} \quad (71)$$

$$\mathbf{r}_{eff}^{(e)} = \mathbf{r}^{(e)} - \mathbf{F}^{(e)} (\mathbf{H}^{(e)})^{-1} \mathbf{h}^{(e)} \quad (72)$$

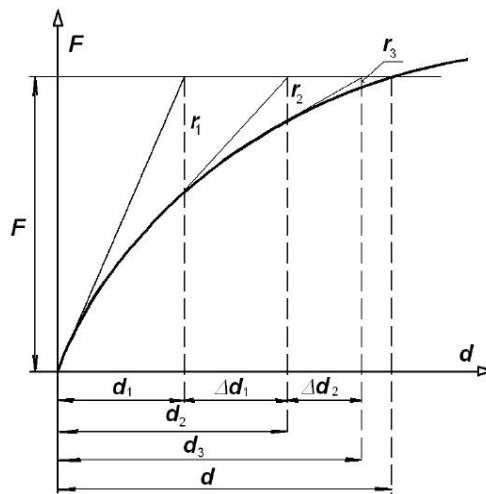


Fig. 11 Newton-Raphson method

5. Numerical simulations

5.1 Quasi-brittle case

We first carry out numerical analysis of a bar of a unit cross-sectional area subjected to constant velocity $v = 15\text{m/s}$ applied at both ends in the outward direction. The geometric and material properties of the bar are $L = 2\text{m}$, $E = 10000\text{MPa}$, $\rho = 1\text{kg/m}^3$, $\sigma_y = 3000\text{MPa}$, $\sigma_u = 3000\text{MPa}$. The numerical results are compared for $t = \frac{0.5L}{c_e} = 0.01\text{s}$ and for $t = \frac{1.5L}{c_e} = 0.03\text{s}$ with analytical results of the elastic solution.

For $t = \frac{0.5L}{c_e} = 0.01\text{s}$, the waves from the left and right have both travelled $1/2$ of the bar, i.e., at this time the two waves have not yet crossed and, therefore, all areas of the bar are elastic in which the bar area of $-L/2 \leq x \leq L/2$ has approximate values of zero of displacement and strain. Propagation of waves from the both ends to the bar's center presented in Fig. 12 is well compatible with these predictions. Meanwhile, a comparison in Fig. 13 shows a good agreement between numerical and analytical solutions.

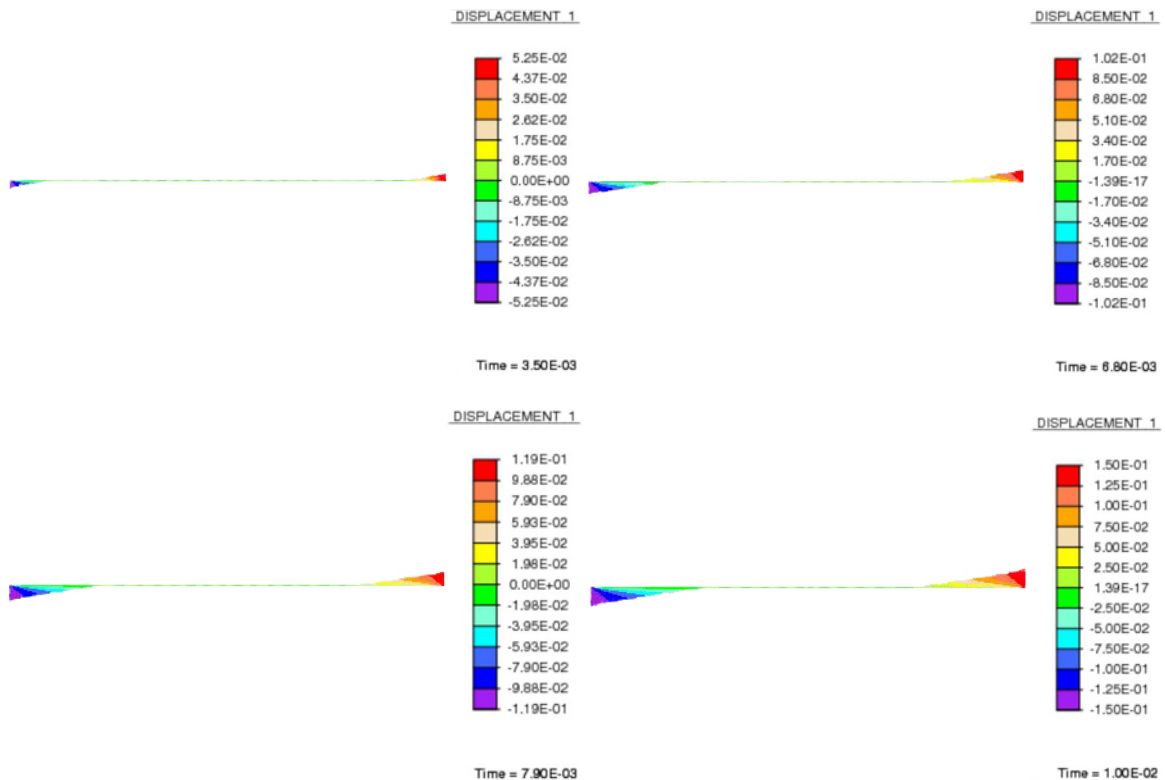


Fig. 12 Wave propagation from the right and left end to the center of the bar at different instants in time

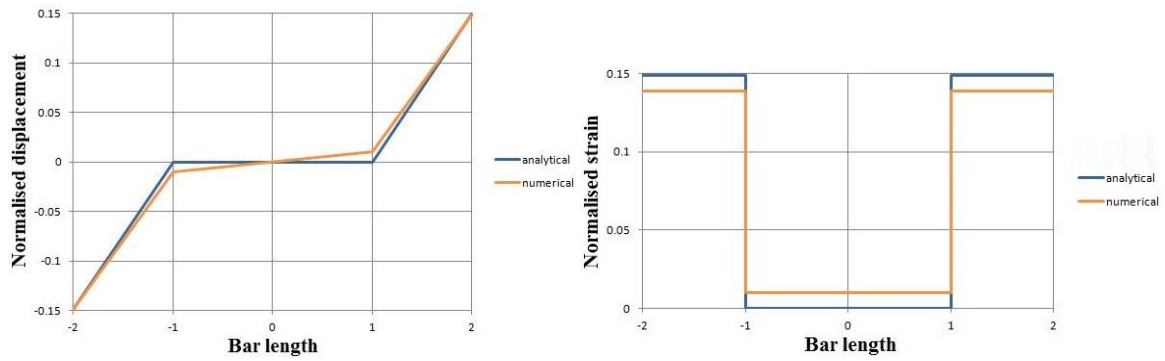


Fig. 13 Comparison between analytical and numerical solution for $t = 0.01s$

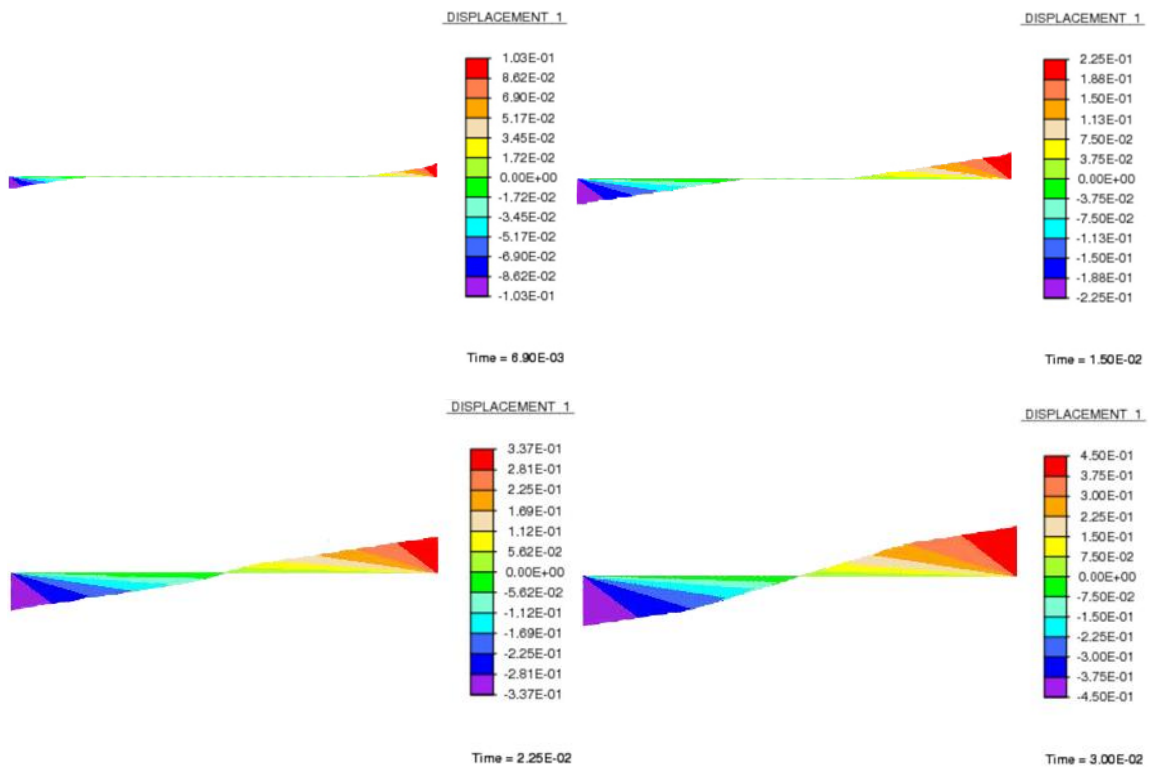


Fig. 14 Wave propagation from the right and left end to the center of the bar at different instants in time

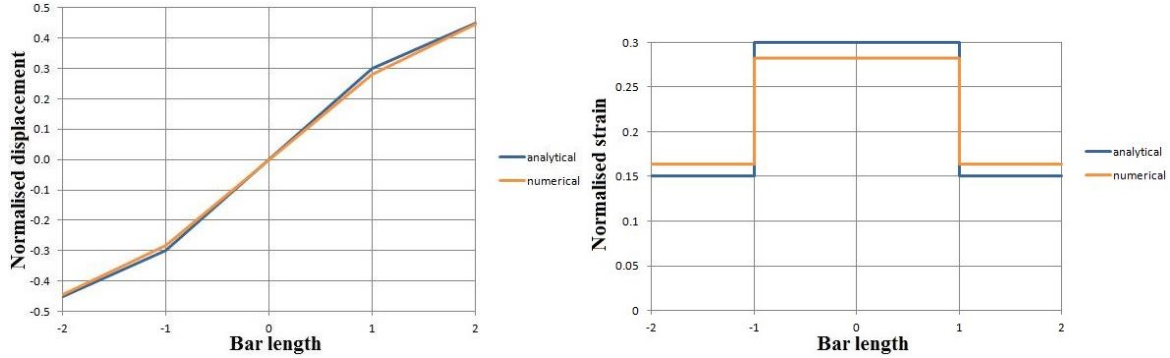


Fig. 15 Comparison between analytical and numerical solution for $t = 0.03s$ and $\epsilon \leq \frac{\epsilon_p}{2}$

At $t = \frac{1.5L}{c_e} = 0.03s$, two step waves from the left and right crossed in the area of $-L/2 \leq x \leq L/2$ and strain doubles instantaneously in this area. Nevertheless, the linear elastic regime still continues happening throughout the complete length of the bar as the stress remains small enough in comparison with the ultimate stress. Wave propagation of the two waves in Fig. 14 follows well these predictions.

Similar to $t = \frac{0.5L}{c_e} = 0.01s$ the difference in results between numerical and analytical solution in case of $t = \frac{1.5L}{c_e} = 0.03s$ is negligible and is obviously showed in Fig. 15.

Next keeping $v = 15m/s$, $L = 2m$, $E = 10000MPa$, $K_s = -2500MPa$, $\rho = 1kg/m^3$ fixed and changing values of yield stress and ultimate stress, $\sigma_y = 900MPa$, $\sigma_u = 880MPa$, respectively. All numerical results will be compared with the analytical results of the strain-softening solution for $t = \frac{1.5L}{c_e} = 0.03s$. At this time, the bar area of $-\frac{L}{2} \leq x \leq \frac{L}{2}$ is governed by the strain-softening solution. The rest of the bar, $-L \leq x < -\frac{L}{2}$ and $\frac{L}{2} < x \leq L$ still maintains the elastic regime.

The Fig. 16(a) illustrates the longitudinal displacement along the bar for different choice of finite element discretization at $t = \frac{1.5L}{c_e}$. A strong sensitivity of results due to mesh discretization is visible in the strain-softening region. Meanwhile, for the remaining elastic domain mesh sensitivity is not present although an improvement in accuracy of results can be seen with finer mesh spacing. The numerical results approach the exact solution with increasing refinement of the mesh size.

The results in Fig. 16(a) agree quite well with the predicted strain-softening behavior for longitudinal displacement. The exact solution predicts that displacement develops a discontinuity at infinitely small area near $x = 0$ with a “jump”. Outside of this area the bar unloads and all displacements accumulate at $x = 0$. The numerical results reflect this strain-softening behavior well. The strain-softening area narrows with increasing the number of element and all displacements accumulate in one element.

Results for longitudinal strain along the bar are exhibited in Fig. 16(b). For the strain-softening

zona strong sensitivity of results can be observed, where as mesh sensitivity is not visible in the remaining elastic domain. However, the accuracy of results rises with finer mesh spacing. The strain measured in the strain-softening elements increases with increasing element number.

The results illustrated in Fig. 16(b) conform to the predicted strain-softening behavior well. Analytically, strain is supposed to be infinite in the strain-softening discontinuity at $x = 0$. Outside the discontinuity the bar unloads and strain gradually reduces to zero. This strain-softening behavior is well represented in the numerical results. The strain-softening element in the middle of the bar undergoes intense deformation. Strain increases with increasing mesh refinement. Strain in elements outside the strain-softening element gradually decreases to zero.

The process in which the two step waves from the right and left boundary travel to the center of the bar in Fig. 17 indicates strain-softening behavior as expected with a displacement jump around an area of $x = 0$. Fig. 18 exhibits typical stress-strain curve for quasi-brittle case. It can be seen that after reaching ultimate stress the stress-strain response “turns down” and material strain softens.

5.2 Quasi-ductile case

Similarly, numerical analysis of a bar of unit cross-sectional area subjected to constant velocity $v = 15$ m/s applied at both ends in the outward direction was performed. The bar has the geometric and material parameters as follows: $L = 2$ m, $E = 10000$ MPa, $K = 10000$ MPa, $K_s = -2500$ MPa, $\rho = 1$ kg/m³, $\sigma_y = 680$ MPa, $\sigma_u = 880$ MPa. Besides, to observe influence of ductility on failure process of material, fixed values of Young’s modulus ($E = 10000$ MPa) and softening modulus ($K_s = -2500$ MPa) together with various values of isotropic hardening modulus K were used. All numerical results of different mesh discretisations are compared for $t = \frac{1.5L}{c_e} = 0.03$ s with exact solution. At this time the waves from the left and right have both travelled $3/2$ of the bar. Accordingly, the bar area of $-\frac{L}{2} \leq x \leq \frac{L}{2}$ is governed by strain-softening regime, whereas the rest of the bar obeys the elastic solution. In addition to elastic and strain-softening regime material undergoes a phase of strain-hardening before failure (see Fig. 21).

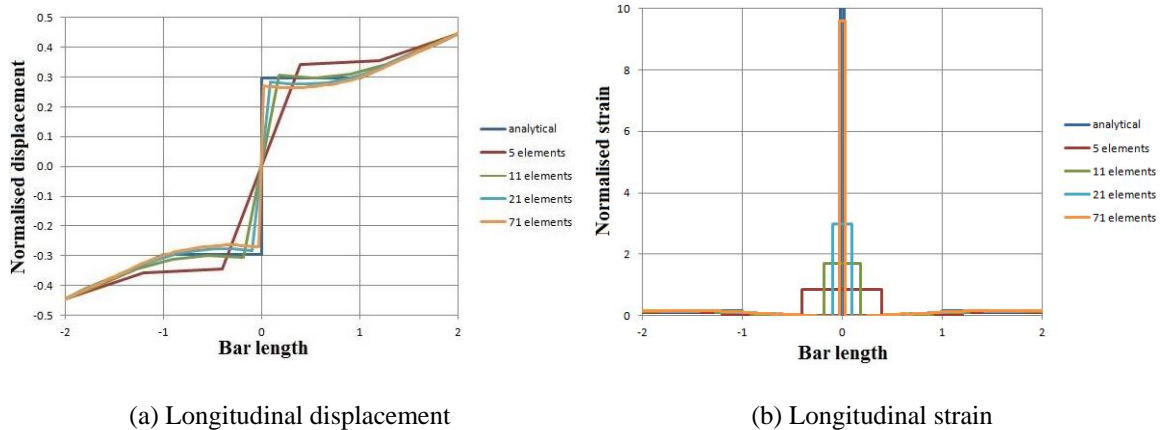


Fig. 16 Comparison between analytical and numerical solution at $t = 0.03$ s and $\frac{\epsilon_p}{2} < \epsilon \leq \epsilon_p$

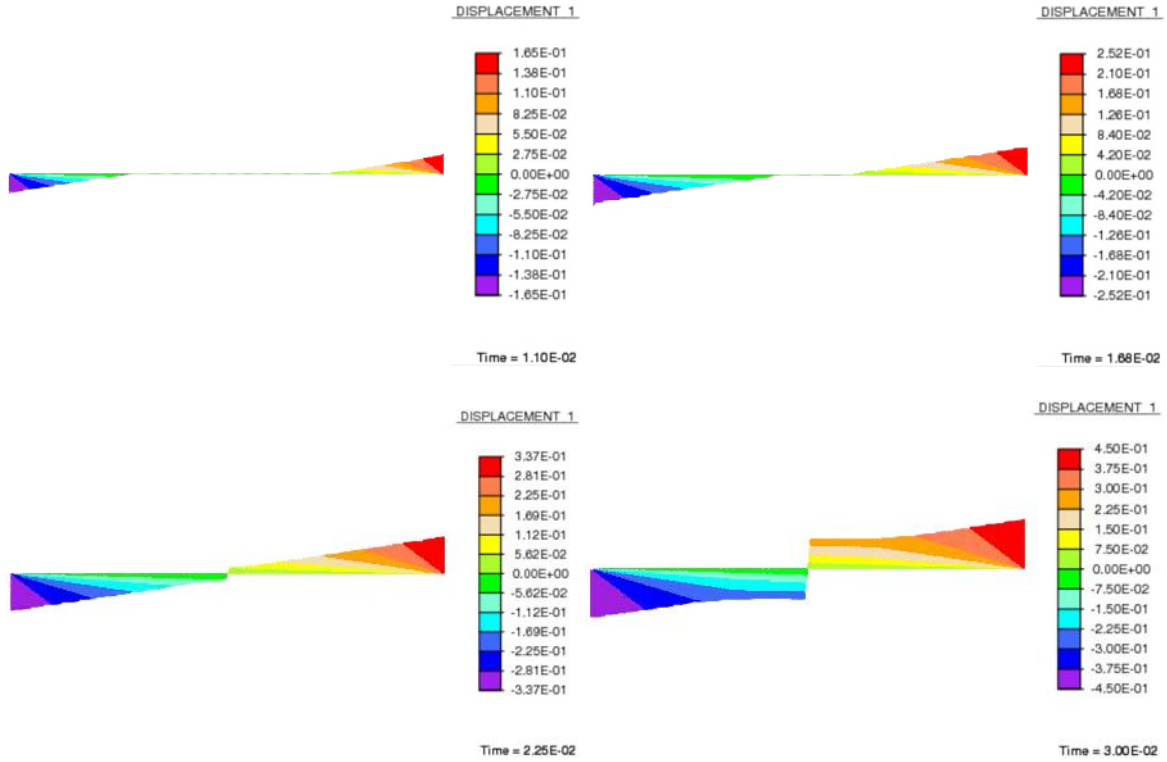


Fig. 17 Wave propagation from the right and left end to the center of the bar at different instants in time

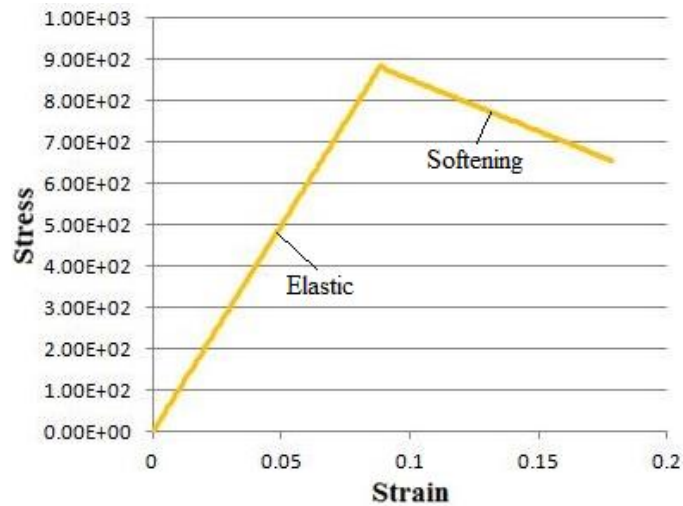


Fig. 18 Typical stress-strain curve for quasi-brittle case

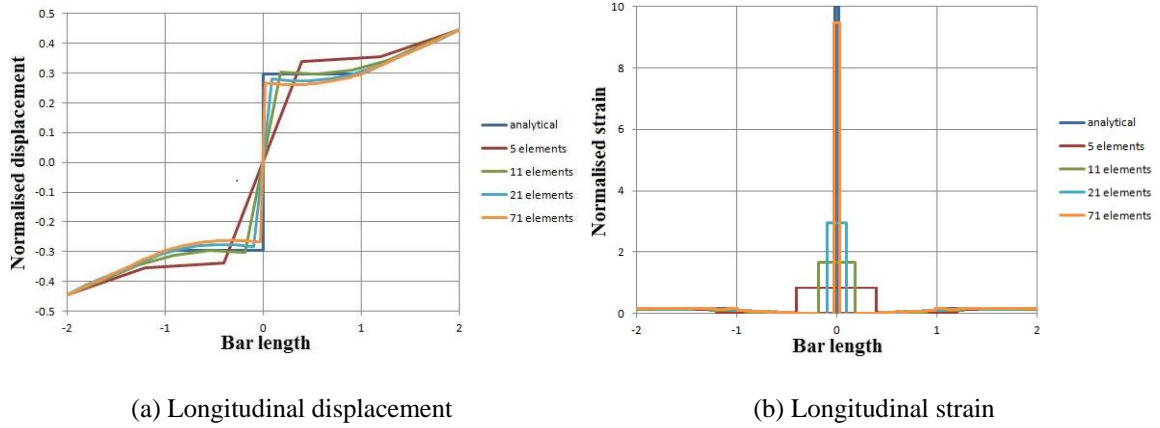


Fig. 19 Comparison between analytical and numerical solution at $t = 0.03s$ and $\frac{\epsilon_p}{2} < \epsilon \leq \epsilon_p$

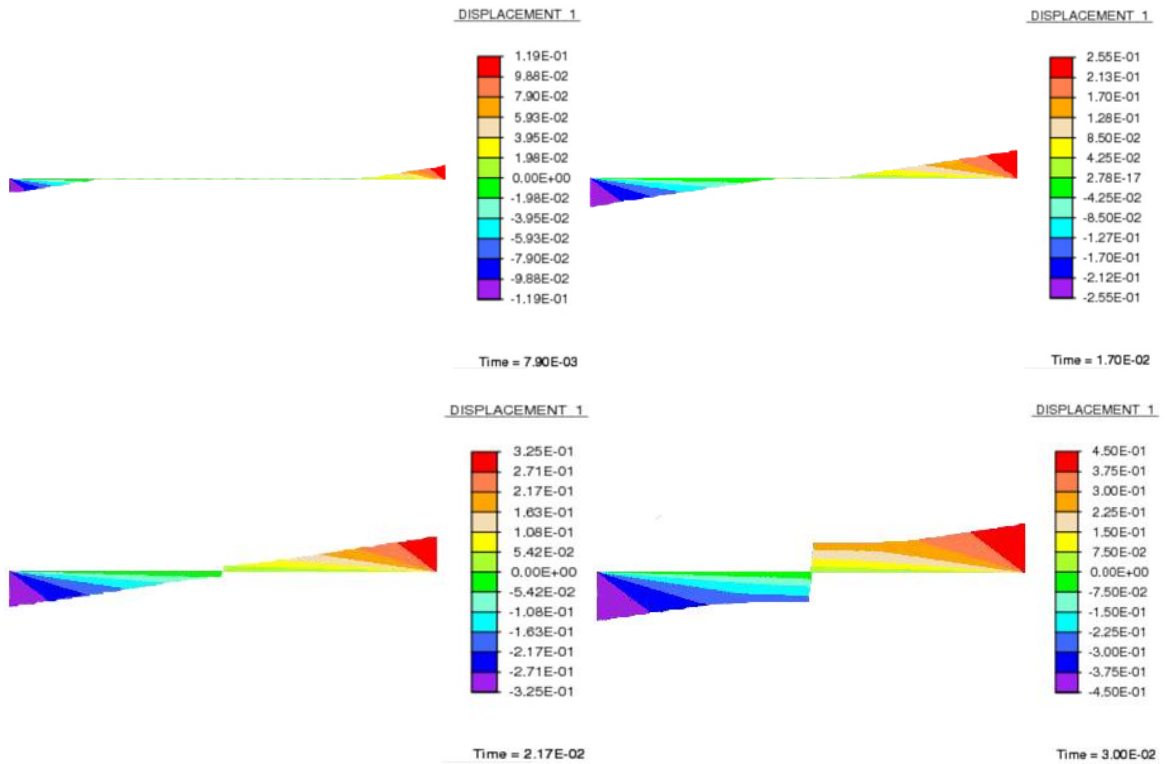


Fig. 20 Wave propagation from the right and left end to the center of the bar at different instants in time

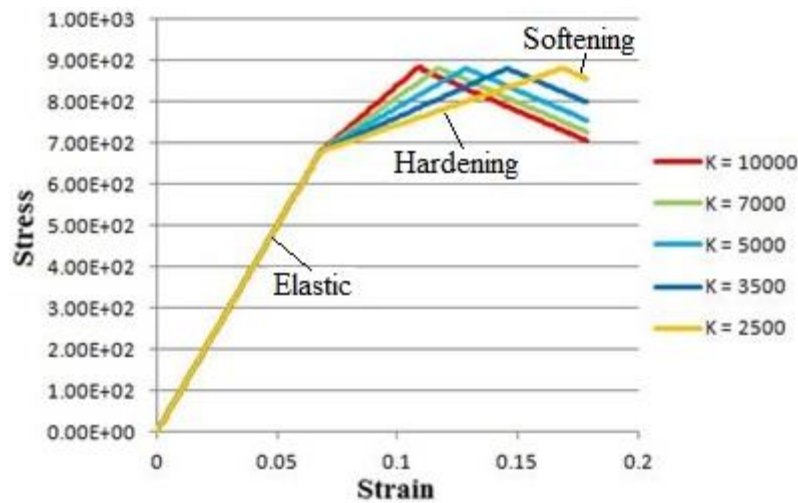


Fig. 21 Typical stress-strain curve for quasi-ductile case

Figs. 19(a) and 19(b) show results for longitudinal displacement and strain, respectively, along the bar. Obviously, there is a strong sensitivity of results on the mesh discretization for the strain-softening zone. Meanwhile, in the remaining elastic domain mesh sensitivity is not present although an improvement in result accuracy can be seen with increasing mesh refinement. The numerical results well coincide with the predicted strain-softening behavior where in a displacement jump occurs and strain is supposed to be infinite in the strain-softening discontinuity at $x = 0$. The bar unloads elastically outside the strain-softening region with accumulation in one element of all displacements and gradual decrease to zero of strain. The numerical results approach the exact solution with increasing the number of element. The strain-softening behavior is clearly exhibited in Fig. 20 via wave propagation according to time.

From the typical stress-strain response presented in Fig. 21 it can be seen that the higher ductility (the smaller isotropic hardening modulus K) the larger plastic deformation material will undergo before failure and, therefore, this also implies the larger area under the stress-strain diagram, i.e., the larger strain energy density at rupture (modulus of toughness). Hence, the material has higher resistance to cracks and crack propagation and is more resistant to fracture. These above characteristics hold for ductile failure regime of material.

6. Conclusions

The aim of this work was to gain a better understanding of strain-softening behavior in discrete models with embedded strong discontinuities. In addition, brittle/ductile failure mode transitions can be captured well with these elements.

A one-dimensional dynamic strain-softening problem by Bazant and Belytschko (1985) was used for the analytical and numerical investigations of simple case without FPZ – fracture process zone. The analytical strain-softening problem is limited to an area with zero width. The strain is infinite in the strain-softening domain. The implementation of the dynamic strain-softening

problem was done with a discrete bar model with strong discontinuities in FEAP. These discontinuities are embedded into the finite element through the proper enhancement of the discrete strain field of the element. It was shown that strain-softening leads to a sensitivity of results on the mesh discretization. Strain localizes in a single element which is the smallest possible area in the finite element simulations. The numerical results depend strongly on the chosen mesh discretization and well approach the analytical strain-softening solution with increasing refinement of the mesh size.

The explorations are also performed for the more general case with the fracture process zone with hardening behavior, which proceeds the strain-softening. This kind of behavior introduces increased ductility in dynamic failure phenomena.

Acknowledgments

This work was supported by the excellence scholarship from Vietnamese Ministry of Education and Training and funding of Chaire de Mécanique Picardie. This support is gratefully acknowledged.

References

- Armero, F. and Linder, C. (2009), "Numerical simulation of dynamic fracture using finite elements with embedded discontinuities", *Int. J. Fracture*, **160**(2), 119-141.
- Bazant, Z.P. and Belytschko, T.B. (1985), "Wave propagation in a strain-softening bar: Exact solution", *J. Eng. Mech. - ASCE*, **111**(3), 381-389.
- Brancherie, D. and Ibrahimbegovic, A. (2009), "Novel anisotropic continuum-discrete damage model capable of representing localized failure of massive structures: Part I: theoretical formulation and numerical implementation", *Eng. Comput.*, **26**(1-2), 100-127.
- Ibrahimbegovic, A. (2009), *Nonlinear Solid Mechanics: Theoretical Formulations and Finite Element Solution Methods*, Springer, Berlin, Germany.
- Ibrahimbegovic, A. and Brancherie, D. (2003), "Combined hardening and softening constitutive model of plasticity: precursor to shear slip line failure", *Comput. Mech.*, **31**(1-2), 88-100.
- Ibrahimbegovic, A., Hajdo, E. and Dolarevic, S. (2013), "Linear instability or buckling problems for mechanical and coupled thermomechanical extreme conditions", *Coupled Syst. Mech.*, **2**(4), 349-374.
- Ibrahimbegovic, A. and Melnyk, S. (2007), "Embedded discontinuity finite element method for modeling of localized failure in heterogeneous materials with structured mesh: an alternative to extended finite element method", *Comput Mech.*, **40**(1), 149-155.
- Lemaitre, J. and Chaboche, J. L. (1988), *Mécanique De Matériaux Solides*, Dunod, Paris, France.
- Neilsen, M.K. and Schreyer, H.L. (1993), "Bifurcations in elastic-plastic materials", *Int. J. Solids Struct.*, **30**(4), 521-544.
- Ngo, V.M., Ibrahimbegovic, A. and Hajdo, E. (2014), "Nonlinear instability problems including localized plastic failure and large deformations for extreme thermomechanical load", *Coupled Syst. Mech.*, **3**(1), 89-110.
- Nikolic, M. and Ibrahimbegovic, A. (2015), "Rock mechanics model capable of representing initial heterogeneities and full set of 3D failure mechanisms", *Comput. Method. Appl. M.*, **290**, 209-227.
- Nikolic, M., Ibrahimbegovic, A. and Miscevic, P. (2015), "Brittle and ductile failure of rocks: Embedded discontinuity approach for representing mode I and mode II failure mechanisms", *Int. J. Numer. Meth. Eng.*, **102**(8), 1507-1526.

- Oliver, J. (1996), "Modelling strong discontinuities in solid mechanics via strain softening constitutive equations. Part 2: numerical simulation", *Int. J. Numer. Meth. Eng.*, **39**(21), 3575-3600.
- Ortiz, M. (1985), "A constitutive theory for inelastic behavior of concrete", *Mech. Mater.*, **4**, 67-93.
- Rudnicki, J. W. and Rice, J. R. (1975), "Conditions for the localization of deformation in pressure-sensitive dilatant materials", *J. Mech. Phys. Solids*, **23**, 371-394.
- Simo, J.C., Oliver, J. and Armero, F. (1993), "An analysis of strong discontinuities induced by strain-softening in rate-independent inelastic solids", *Comput. Mech.*, **12**(5), 277-296.
- Taylor, R., *FEAP Finite Element Analysis Program*, University of California: Berkeley. (Available from <http://www.ce.berkeley.edu/rft/>).